Talanta 244 (2022) 123383

Contents lists available at ScienceDirect

Talanta

journal homepage: www.elsevier.com/locate/talanta

Laser tweezers Raman spectroscopy combined with deep learning to classify marine bacteria

Bo Liu [a,b], Kunxiang Liu [a,b], Nan Wang [c], Kaiwen Ta [d], Peng Liang [a,b], Huabing Yin [e], Bei Li [a,b,*]

[a] State Key Laboratory of Applied Optics, Changchun Institute of Optics, Fine Mechanics and Physics, Chinese Academy of Sciences, Changchun, 130033, PR China
[b] University of Chinese Academy of Sciences, Beijing, 100049, PR China
[c] Hooke Instruments Ltd, Changchun, 130033, PR China
[d] Institute of Deep Sea Science and Engineering, Chinese Academy of Sciences, Sanya, Hainan, 572000, China
[e] James Watt School of Engineering, University of Glasgow, G12 8LT, UK

ARTICLE INFO

Keywords:
Progressive generative adversarial network
Residual network
Raman spectroscopy
Optical tweezers
Classification
Deep-sea microorganism

ABSTRACT

Rapid identification of marine microorganisms is critical in marine ecology, and Raman spectroscopy is a promising means to achieve this. Single cell Raman spectra contain the biochemical profile of a cell, which can be used to identify cell phenotype through classification models. However, traditional classification methods require a substantial reference database, which is highly challenging when sampling at difficult-to-access locations. In this scenario, only a few spectra are available to create a taxonomy model, making qualitative analysis difficult. And the accuracy of classification is reduced when the signal-to-noise ratio of a spectrum is low. Here, we describe a novel method for categorizing microorganisms that combines optical tweezers Raman spectroscopy, Progressive Growing of Generative Adversarial Nets (PGGAN), and Residual network (ResNet) analysis. Using the optical Raman tweezers, we acquired single cell Raman spectra from five deep-sea bacterial strains. We randomly selected 300 spectra from each strain as the database for training a PGGAN model. PGGAN generates a large number of high-resolution spectra similar to the real data for the training of the residual neural network. Experimental validations show that the method enhances machine learning classification accuracy while also reducing the demand for a considerable amount of training data, both of which are advantageous for analyzing Raman spectra of low signal-to-noise ratios. A classification model was built with this method, which reduces the spectra collection time to 1/3 without compromising the classification accuracy.

1. Introduction

Marine litter in the ocean has received much attention in recent decades. The importance of bacteria in marine debris, including some potentially beneficial microorganisms for the ecosystem, cannot be overlooked [1]. However, few methods exist for identifying microorganisms in marine litter. The majority of traditional methods involve complicated sample processes and are destructive [2]. For example, living cells must be lysed to extract DNA or proteins for identification. In addition, these methods are difficult to use for in-situ identification, limiting the exploration of the real-world samples [3]. As a result, methods for rapid, culture-free, non-destructive microbial identification at the single-cell level are required. Raman spectroscopy is a non-invasive method to identify single microbial cells in situ and study their metabolism [4]. Single-cell Raman spectra contain abundant biochemical information of bacteria, thus have been used as a "chemical fingerprint" for bacterial species identification [5]. However, spontaneous Raman signals of biological molecules are very weak due to the low Raman scattering efficiency (10^{-8} scattering probability) [6] and susceptibility to interference from (auto)fluorescence. Therefore, long Raman acquisition ranging from 1 s to 10s' seconds from immobilized cells is often needed [7–9], which could compromise cell viability.

Acquiring spectra of cells in liquid is preferred but facing challenges associated with Brownian motion and cell motility. These difficulties have been solved with the advent of optical tweezers. Optical tweezers employ a highly concentrated laser beam to apply pNs optical stresses to single cells, allowing them to be trapped and manipulated [10,11]. Xie et al. realized the combination of Raman spectroscopy and optical

* Corresponding author. State Key Laboratory of Applied Optics, Changchun Institute of Optics, Fine Mechanics and Physics, Chinese Academy of Sciences, Changchun, 130033, PR China
E-mail address: beili@ciomp.ac.cn (B. Li).

https://doi.org/10.1016/j.talanta.2022.123383
Received 21 November 2021; Received in revised form 5 March 2022; Accepted 11 March 2022
Available online 16 March 2022

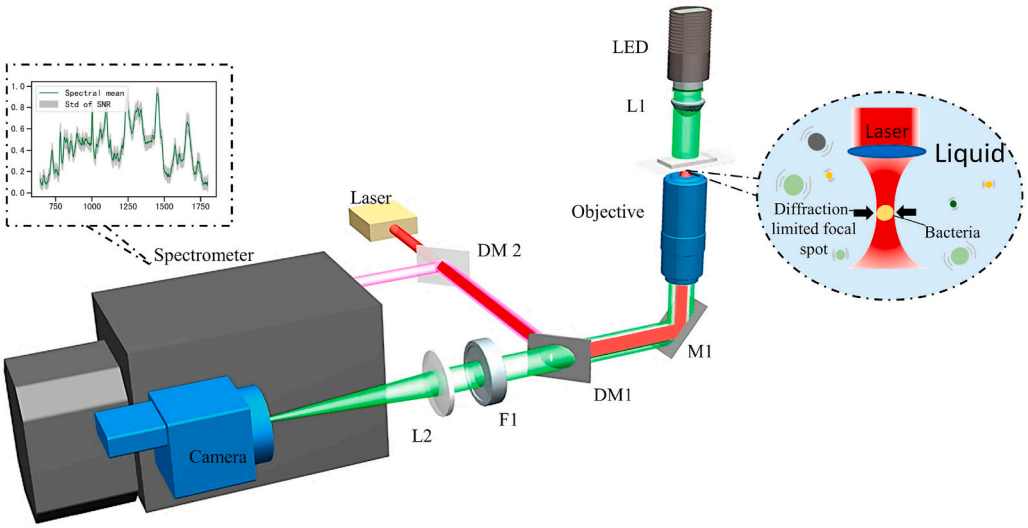

Fig. 1. LTRS setup. The red path represents the 785 nm laser beam, which is utilized as both an optical tweezer and a Raman excitation beam. The pink route indicates Raman scattering of the material. Green represents real-time imaging light in confocal microscopy (Optical component abbreviations in Supplementary Information Table S1). Conceptual measurement schematic: Single cells can be captured and Raman signals obtained by focusing the exciting laser source to a spot size with limited diffraction. (For interpretation of the references to colour in this figure legend, the reader is referred to the Web version of this article.)

tweezers technology for cell classification without damaging them [12].

Conventional multivariate analytic methods, including principal component analysis (PCA), hierarchical cluster analysis (HCA), linear discriminant analysis (LDA), K-Nearest Neighbor (KNN), and nonlinear support vector machine (SVM), are frequently utilized for the classification of Raman spectra [4]. Linear models (PCA-LDA) have been the most popular [13–15]. However, the spectral response to the substance is not linear due to sample variations, acquisition settings, and instruments, resulting in reduced precision of the model's prediction. SVM is regarded as superior to the others, but its accuracy is affected when processing massive data sets and a high number of classes [16]. Complex procedures, poor performance, and limited robustness remain prevalent challenges in most Raman classification approaches. Furthermore, variations in microbial Raman spectra are subtle and can be easily masked by the background noise [17]. To obtain high identification accuracy, a high signal-to-noise ratio (SNR) is necessary, usually requiring a long acquisition.

Deep learning has shown significant benefits in the image processing [18], speech recognition [19], and natural language processing [20]. It can extract hidden features from the original data and offers an end-to-end feature extraction [21]. Deep learning can reduce nonlinear effects and improve the model interpretability [22]. Lu et al. combined laser tweezers Raman Spectroscopy with convolutional neural network (CNN) for microbial identification [9]. Ho et al. demonstrated that ResNet could accurately classify Raman spectra with very low SNRs [8]. However, such models still necessitate a large number of reference data for the training [23].

Compared to CNN-based supervised algorithms, Semi-supervised methods based on generative adversarial networks (GAN) can deliver accurate taxonomic results with fewer samples [24]. Teng et al. discovered that the GAN-based spectrum generation method could expand the spectrum database effectively [25]. Yu et al. confirmed that GAN could produce Raman spectra similar to those of real samples [26]. However, the generation of high-resolution Raman spectral images via GANs is not stable – this limitation has been recently addressed using Progressive Growing of Generative Adversarial Nets (PGGAN) [27].

Here, we developed a new approach for classifying bacteria by coupling laser tweezers Raman spectroscopy (LTRS) with PGGAN and ResNet. Via optical tweezers Raman spectroscopy, we acquired Raman spectra of individual bacteria cells, which were used in PGGAN to generate a large amount of high-resolution Raman spectra to train ResNet and generate a taxonomic model. This approach does not require collecting a significant quantity of experimental spectra and addresses the issues associated with low SNRs.

2. Materials and methods

2.1. Test materials and screening

Peng et al. (2019) reported that large debris dumps were prevalent in the Xisha Trough region in the northern South China Sea [28]. The manned submersible found a pile of Polyethylene (PE) debris in a submarine canyon northwest of the South China Sea, about 150 km from the nearest coast. This plastic debris is mainly located in two large scouring areas in the steep middle reaches of the canyon [29]. The PE debris samples were collected using the manipulators in the manned submersible Shenhaiyongshi during cruises of R/V TS07. The human-occupied vehicle (HOV) Shenhaiyongshi was developed by the China Shipbuilding Industry Corporation and delivered to the Institute of Deep-sea Science and Engineering, the Chinese Academy of Sciences. Approximately 1 g of the PE debris was first used for cell cultivation using a seawater simulated medium, resulting in a mixture of the microbial community. This mixture was further cultured in a liquid medium and on an agar plate in the presence of a PE film (YiYao, China) to enrich PE-enrich bacteria. Each piece of the PE film is 50 × 50 mm size and 0.25 g (10 pieces were used) and was sterilised in 70% ethanol for 30 min thoroughly washed before use. The culture medium consists of 0.05% yeast extract, 0.2% $(NH_4)_2SO_4$, 2.6% NaCl, 0.05% KCl, 0.3% Na_2HPO_4, 0.2% KH_2PO_4 and 1% trace elements (0.1% $FeSO_4 \cdot 7H_2O$, 0.1% $MgSO_4 \cdot 7H_2O$, 0.01% $CuSO_4 \cdot 5H_2O$, 0.01% $MnSO_4 \cdot 5H_2O$, and 0.01% $ZnSO_4 \cdot 7H_2O$) in 10 mM phosphate buffer (pH 7.5). Cultures were incubated at 30°C, 250 rpm. Visible colonies were further purified several times. The purity of five bacterial strains was confirmed by a repeated 16S rRNA sequencing [30].

2.2. Sequencing and phylogenetic analysis

After cells were cultured into the late log phase, DNA was extracted from cells using the Bacterial DNA Kit (Omega, D3350, USA). The quality of extracted DNA was checked by 1% agarose gel electrophoresis and spectrophotometry (optical density at 260 nm/280 nm ratio). The 16S rRNA gene sequence was amplified with the Bacteria primer set 27F (AGAGTTTGATCMTGGCTCAG) and 1492R (TACGGYTACCTTGTTACGACTT). Sequencing was performed using the Illumina ABI 3730XL sequencing platform (Illumina, Inc., CA, USA). Raw sequencing data were processed using the pipeline tools QIIME (version v.1.8.0) and MOTHUR (version v.1.30.1). The obtained sequences were aligned with organisms present in the GenBank database using the BLAST field [30]. Genome sequences of *Halomonas* sp., *Pseudomonas* sp.,

Acinetobacter sp., *Fictibacillus* sp., and *Staphylococcus* sp. have been deposited at GenBank under the accession numbers OK632277, OK632278, OK632279, OK632280 and OK632281. Some of those bacteria can grow on the surface of PE materials, suggesting a potential ability of these microorganisms to utilize, at least partly, PE as a potential carbon source. The sequence reads have been deposited at the NCBI Short Read Archive (SRA) under the accessions SUB10570764.

2.3. LTRS system

To obtain the Raman spectra of various microorganisms at the single-cell level, we built up a laser tweezers Raman spectroscope, which combines a confocal Raman spectrometer with optical tweezers. The schematic diagram of our LTRS system is shown in Fig. 1. The system consists of an optical tweezer laser, a confocal Raman spectrometer, an imaging system, and other optical components. The laser beam emitted by a 785 nm continuous laser with adjustable power (I0785SU0100PA; 785 nm; IPS) is guided to the objective lens (LUNOLFLN40XW; numerical aperture = 0.8; Olympus) through Dichroic mirrors (DM1, DM2) and mirror (M1), forming a single-beam gradient force optical trap. The same laser beam was used to excite Raman scattering of the captured microbial cells. The Raman scattering focuses on the commercial confocal Raman spectrometer entrance through the reflector and dichroic mirrors.

The confocal Raman spectrometer is equipped with an 1800 grooves/mm grating and projects the Raman scattered light on a thermoelectric-cooled CCD camera (2000 × 256 pixel; iVac316; ANDOR). The LED emits green light with a wavelength of 550 nm, which is irradiated on the sample by an aspheric mirror, and the transmitted light passes through the objective lens to form parallel light. The parallel light is reflected by the reflector lens and dichroic mirror and then further converged through the imaging lens onto the CCD camera. We use a short-pass filter to block laser light in front of the camera to prevent laser-induced camera damage.

2.4. Data processing

The Raman spectral signal will be affected by the drift of the excitation laser, the thermal stability noise of the CCD detector, the thermal noise in the electronic circuit, etc. In addition, the position and orientation of the sample placement will also make the spectral signal mixed with noise, which will interfere with the valuable information of the spectrum and affect the prediction effect. Therefore, pre-processing of the obtained raw Raman spectral signal is needed. We removed cosmic rays from the spectrum. We use the "subbackmod" function in the Biodata toolbox [31] for baseline correction, and we use the "mapminmax" function for normalization. Examples of raw and preprocessed spectra are shown in Fig. S1.

After pre-processing, the spectra are fitted using PGGAN, and 1000 high-resolution Raman spectra similar to the experimental ones are generated after sufficient interaction training. The 1000 spectra generated are fed into ResNet and sufficiently trained to obtain an accurate classification model.

3. Results and discussion

3.1. Raman Spectroscopy acquisition

Raman spectra of individual cells randomly selected from five bacterial strains were collected, including *Acinetobacter* sp., *Fictibacillus* sp., *Halomonas* sp., *Pseudomonas* sp., and *Staphylococcus* sp. To reduce the effect of spectral noise, at least 300 single cell Raman spectra from each bacterial strain were randomly selected as the training data set for the PGGAN model. To reduce the interference of the culture medium, cells are centrifuged and washed with DI water for Raman spectrum acquisition. Each cell is excited for 10 s at a power of 30 mW after the objective (Fig. 2).

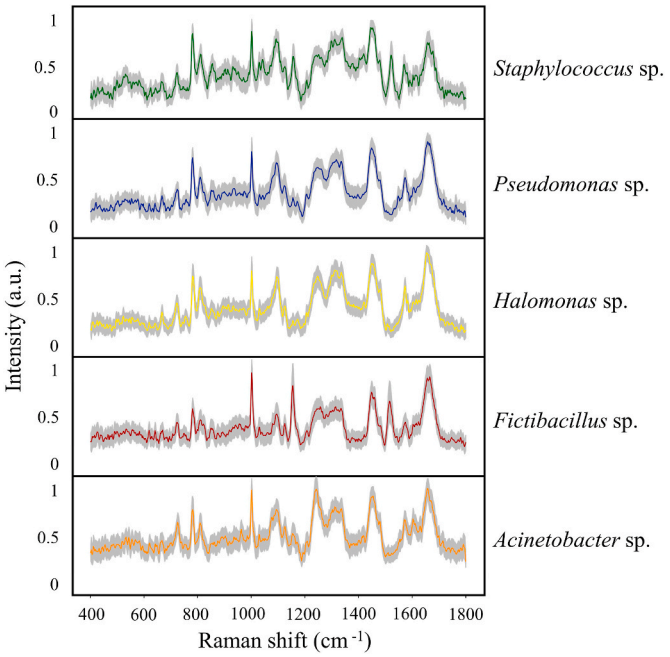

Fig. 2. Raman spectra of five marine microorganisms. LTRS obtained at least 300 spectra for each strain. The solid line represents the average value of the Raman spectrum, and the standard deviation is represented by shadow.

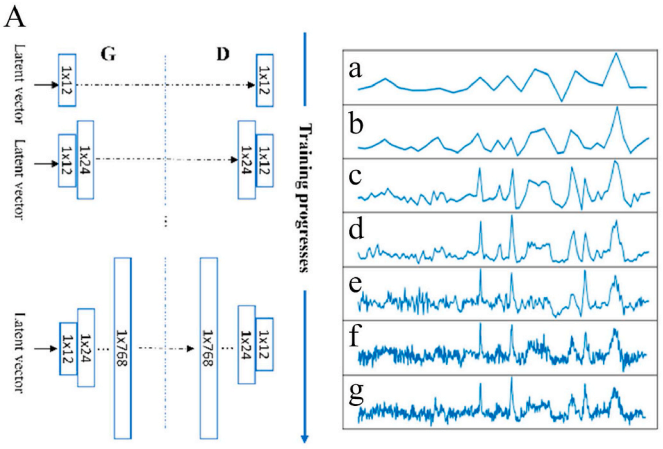

Fig. 3. (A) PGGAN process training to *Fictibacillus* sp. (B) Spectra obtained from low to high resolution after training. a. 24 pixels; b. 48 pixels; c. 96 pixels; d. 192 pixels; e. 384 pixels; f. 768 pixels; g. Real spectra were obtained using a Raman spectrometer.

3.2. Data generation of PGGAN

We trained our networks according to the setup described by Kay Gregor Hartmann et al. [32]. PGGAN consists of a generator G and a discriminator D, which compete to improve performance based on the available training data. The generator consists of a fully connected layer and 6 up-sampling blocks, each of which contains 1 up-sampling layer and 2 convolutional layers of size 9. The discriminator consists of 6 discriminant blocks, each containing 2 convolutional layers of size 9 and 1 down-sampling layer. We use leaky ReLU [33] in the discriminator and generator. 2000 epochs were trained at each resolution stage, and an additional 2000 epochs were trained at each stage for fading. ADAM optimizer [34] was used to train the network, using the following

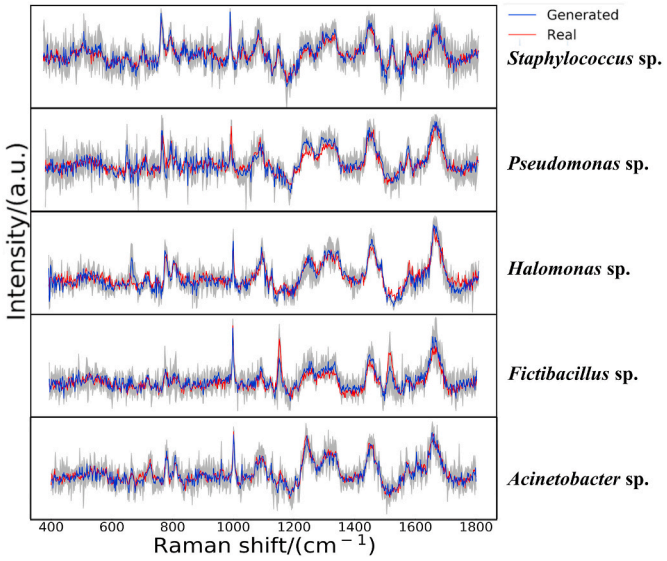

Fig. 4. Comparison between the generated and the real spectra: the blue line is the generated spectrum. The red line is the real spectrum. The grey shaded part is the area formed by the maximum and minimum values of the generated spectrum. (For interpretation of the references to colour in this figure legend, the reader is referred to the Web version of this article.)

parameters: the learning rate at 0.001; exponential decay rates at $\beta_1 = 0$ and $\beta_2 = 0.99$. We started with low-resolution images and gradually increased the resolution by adding layers to the network (Fig. 3A). This progressive nature enables the training to find the image distribution's large-scale structure before focusing on smaller-scale characteristics [27]. The generated spectrum is getting closer and closer to the real one as the number of training sessions increases (Fig. 3B, a-f). As shown in Fig. 4, for each strain, the average spectra of the generated spectra and the real spectra are indistinguishable by the naked eye.

Collecting 1000 experimental Raman spectra would take a skilled researcher about 10 h. In contrast, we only need to acquire 300 experimental Raman spectra (i.e. 3 h) to generate 1000 spectra of equivalent quality for modelling. Although generating the spectra takes about 2 h, the program runs automatically without supervision.

3.3. ResNet taxonomic model identifies microbial species with high accuracy

The CNN architecture is adapted from the ResNet architecture [35], which has been used in various computer vision tasks. ResNet can provide high accuracy when classifying low SNR Raman spectra [8]. Fig. 5 shows a block diagram of the network, including an initial convolution layer, six residual layers, and a fully connected (fc) classification layer. We trained our networks according to the setup described by Ho C S [8]. We use the Adam optimizer across all experiments [34].

To evaluate the effectiveness of the classification model and avoid the problems caused by unreasonable data set partitioning, we introduce a 5-fold cross-validation method. First, we divided the data of each bacterium into 5 sub-groups equally. Four groups were used to train the classification model, and one group was used as the test data. To prevent the neural network from overfitting, the data of all four groups were further randomly recombined into two parts:80% data for training and 20% data for validation. These generated five ResNet classification models. Through this cross-validation, the model with the highest accuracy is selected as the final model.

Using receiver operating characteristic (ROC) curves, we assessed the specificity and sensitivity of classifying the five strains (Fig. S2). The AUC (area under the ROC curve) of all five strains is greater than 0.99, indicating that our ResNet model has high specificity and sensitivity for classifying different bacterial species. During the ResNet training process, we drew the loss and accuracy curves simultaneously (Fig. S3). The training and validation losses have converged, and the difference between them is small, reaching a good fit.

We used the trained ResNet taxonomic model to classify each bacterial cell in the test dataset. The trained ResNet taxonomic model predicts each test set and assigns it to a species category. Our ResNet taxonomic model used the average value to identify a bacterial species with an accuracy of 99.8 ± 0.2%. As shown in Fig. 6, *Fictibacillus* sp., *Halomonas* sp., *Pseudomonas* sp., *Staphylococcus* sp., and *Acinetobacter* sp.

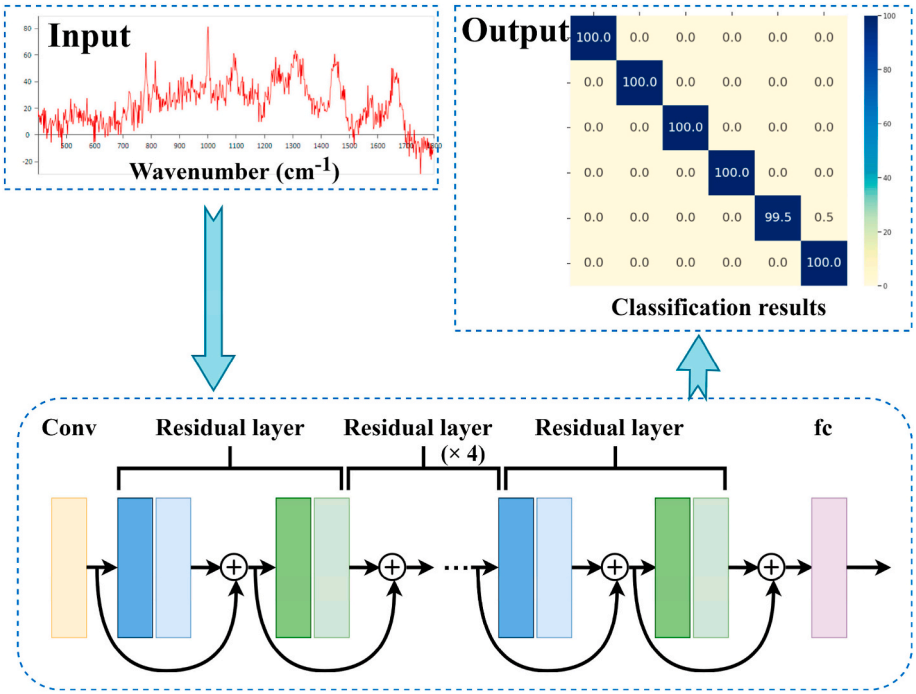

Fig. 5. Deep learning model architecture. A one-dimensional residual network with a total of 25 convolutional layers was used.

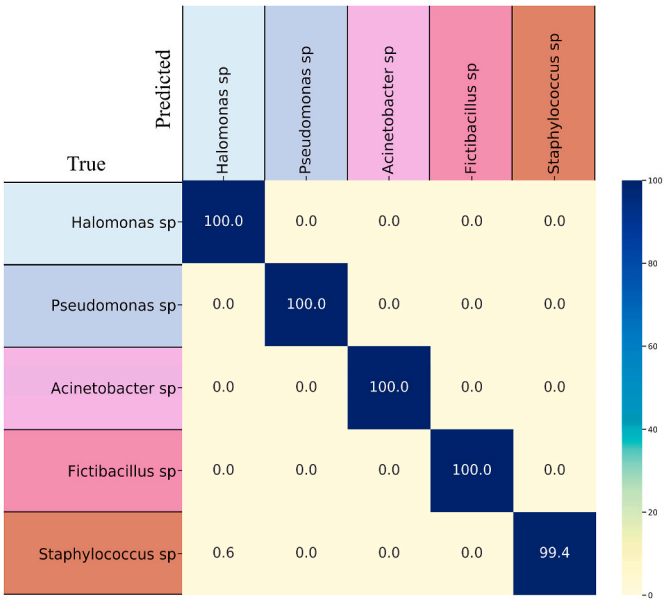

Fig. 6. Results of prediction of five bacterial strains achieved by the ResNet taxonomic model.

have been identified with great accuracy. In comparison, when linear discriminant analysis (PCA-LDA), support vector machine (PCA-SVM) and KNN were used, the accuracy rates were 98 ± 2%, 98 ± 2%, and 95 ± 5%, respectively (Figs. S4A, B, C). In addition, with the CNN model alone, the classification accuracy reached 97 ± 3% (Fig. S5A). However, we combined the model obtained by PGGAN and CNN to predict cell type and successfully achieved a classification accuracy of 98 ± 2% (Fig. S5B). Meanwhile, the ROC curve of the models was calculated (Figs. S5C and D). It is worth noting that PGGAN can also be combined with other deep learning methods to improve classification accuracy. These results demonstrate that Raman spectroscopy, combined with PGGAN and ResNet, can accurately identify microorganisms at the single-cell level.

4. Conclusions

This study presents a novel method for bacterial identification using PGGAN and ResNet combined with laser tweezers Raman spectroscopy. We show that PGGAN can rapidly generate a large number of high-resolution Raman spectra for most existing deep learning approaches and increase their prediction accuracy. Via this approach, only 1/3 of the total spectra need to be experimentally acquired and thus significantly reducing time and labour. ResNet can accurately classify Raman spectra with low SNRs. When combined with PGGAN's high-resolution data, ResNet can quickly, efficiently, and accurately classify single cell Raman spectra.

Our method provides an effective means to solve the challenges associated with the need for substantial training data and Raman spectra of low SNRs. Currently, this technique illustrates the ability to rapidly identify individual bacterial cells in solution without detrimental effects on cells. It is envisaged that when combined with microfluidics, it would allow for fast, accurate, and non-invasive cell sorting. Importantly, this approach doesn't need complicated sample treatments and thus holds great potential for challenging in-situ investigations, such as microbial identification and sorting, benefitting a wide range of microbiology and healthcare areas.

Credit author statement

Bo Liu: investigation, formal analysis, writing - original draft, Writing - review & editing. **Kunxiang Liu**: Analyzed data. **Nan Wang**: resources. **Kaiwen Ta**: sample preparation. **Peng Liang:** resources. **Huabing Yin**: discussion, writing – review & editing. **Bei Li**: Conceptualization.

Declaration of competing interest

The authors declare that they have no known competing financial interests or personal relationships that could have appeared to influence the work reported in this paper.

Acknowledgements

We thank Drs. Chunyang Zhou for helpful discussions. This research was financially supported by the Strategic Priority Research Program of the Chinese Academy of Sciences (No. XDA22020403); the National Natural Science Foundation of China (grants 42006061).

Appendix A. Supplementary data

Supplementary data to this article can be found online at https://doi.org/10.1016/j.talanta.2022.123383.

References

[1] R. Gao, C. Sun, A marine bacterial community capable of degrading poly(ethylene terephthalate) and polyethylene, J. Hazard Mater. 416 (2021) 125928.
[2] X.Y. Wei, X.H. Zhao, Advances in typing and identification of foodborne pathogens, Curr. Opin. Food Sci. 37 (2021) 52–57.
[3] P. Sanmartin, A. DeAraujo, A. Vasanthakumar, Melding the old with the new: trends in methods used to identify, monitor, and control microorganisms on cultural heritage materials, Microb. Ecol. 76 (1) (2018) 64–80.
[4] Z. Guo, M. Wang, A.O. Barimah, Q. Chen, H. Li, J. Shi, H.R. El-Seedi, X. Zou, Label-free surface enhanced Raman scattering spectroscopy for discrimination and detection of dominant apple spoilage fungus, Int. J. Food Microbiol. 338 (2021) 108990.
[5] R.J. Swain, M.M. Stevens, Raman microspectroscopy for non-invasive biochemical analysis of single cells, Biochem. Soc. Trans. 35 (Pt 3) (2007) 544–549.
[6] X. Wang, G. Liu, M. Xu, B. Ren, Z. Tian, Development of weak signal recognition and an extraction algorithm for Raman imaging, Anal. Chem. 91 (20) (2019) 12909–12916.
[7] J. Lukose, M. N, G. Mohan, S. Shastry, S. Chidangil, Optical tweezers combined with micro-Raman investigation of alcohol-induced changes on single, live red blood cells in blood plasma, J. Raman Spectrosc. 50 (10) (2019) 1367–1374.
[8] C.S. Ho, N. Jean, C.A. Hogan, L. Blackmon, S.S. Jeffrey, M. Holodniy, N. Banaei, A. A.E. Saleh, S. Ermon, J. Dionne, Rapid identification of pathogenic bacteria using Raman spectroscopy and deep learning, Nat. Commun. 10 (1) (2019) 4927.
[9] W. Lu, X. Chen, L. Wang, H. Li, Y.V. Fu, Combination of an artificial intelligence approach and laser tweezers Raman spectroscopy for microbial identification, Anal. Chem. 92 (9) (2020) 6288–6296.
[10] T. Tao, J. Li, Y. Lin, Three dimensional manipulation of cells using holographic optical tweezers, Appl. Mech. Mater. 241–244 (2012) 513–516.
[11] M. Woerdemann, C. Alpmann, M. Esseling, C. Denz, Advanced optical trapping by complex beam shaping, Laser Photon. Rev. 7 (6) (2013) 839–854.
[12] C. Xie, M.A. Dinno, Y.Q. Li, Near-infrared Raman spectroscopy of single optically trapped biological cells, Opt. Lett. 27 (4) (2002) 249–251.
[13] J. Chan, D. Taylor, S. Lane, T. Zwerdling, J. Tuscano, T.J.A.C. Huser, Non-destructive identification of individual Leukemia cells by optical trapping Raman spectroscopy, February 9, Anal. Chem. 80 (6) (2007), 80(UCRL-JRNL-229152.
[14] I. Notingher, G. Jell, P.L. Notingher, I. Bisson, O. Tsigkou, J.M. Polak, M. M. Stevens, L.L. Hench, Multivariate analysis of Raman spectra for in vitro non-invasive studies of living cells, J. Mol. Struct. 744–747 (2005) 179–185.
[15] C. Hanson, M. Sieverts, E. Vargis, Effect of principal component analysis centering and scaling on classification of mycobacteria from Raman spectra, Appl. Spectrosc. 71 (6) (2017) 1249–1255.
[16] L. Pan, P. Pipitsunthonsan, C. Daengngam, S. Channumsin, S. Sreesawet, M. Chongcheawchamnan, Method for classifying a Noisy Raman spectrum based on a wavelet transform and a deep neural network, IEEE Access 8 (2020) 202716–202727.
[17] H.J. Butler, L. Ashton, B. Bird, G. Cinque, K. Curtis, J. Dorney, K. Esmonde-White, N.J. Fullwood, B. Gardner, P.L. Martin-Hirsch, M.J. Walsh, M.R. McAinsh, N. Stone, F.L. Martin, Using Raman spectroscopy to characterize biological materials, Nat. Protoc. 11 (4) (2016) 664–687.
[18] M.H. Hesamian, W. Jia, X. He, P. Kennedy, Deep learning techniques for medical image segmentation: achievements and challenges, J. Digit. Imag. 32 (4) (2019) 582–596.
[19] H.M. Fayek, M. Lech, L. Cavedon, Evaluating deep learning architectures for speech emotion recognition, Neural Network. 92 (2017) 60–68.

[20] T. Young, D. Hazarika, S. Poria, E. Cambria, Recent trends in deep learning based natural language processing, IEEE Comput. Intell. Mag. 13 (3) (2018) 55–75.
[21] M. He, X. Li, Y. Zhang, J. Zhang, W. Wang, Hyperspectral image classification based on deep stacking network, in: 2016 IEEE International Geoscience and Remote Sensing Symposium (IGARSS), IEEE, 2016, pp. 3286–3289.
[22] H. Choi, Persistent hidden states and nonlinear transformation for long short-term memory, Neurocomputing 331 (2019) 458–464.
[23] H.-J. Jeong, K.-S. Park, Y.-G. Ha, Image preprocessing for efficient training of YOLO deep learning networks, in: 2018 IEEE International Conference on Big Data and Smart Computing (BigComp), 2018, pp. 635–637.
[24] I.J. Goodfellow, J. Pouget-Abadie, M. Mirza, B. Xu, D. Warde-Farley, S. Ozair, A. Courville, Y. Bengio, Generative adversarial nets, Adv. Neur. In. 27 (2014) 2672–2680.
[25] G.E. Teng, Q.Q. Wang, J.L. Kong, L.Q. Dong, X.T. Cui, W.W. Liu, K. Wei, W. T. Xiangli, Extending the spectral database of laser-induced breakdown spectroscopy with generative adversarial nets, Opt Express 27 (5) (2019) 6958–6969.
[26] S. Yu, H. Li, X. Li, Y.V. Fu, F. Liu, Classification of pathogens by Raman spectroscopy combined with generative adversarial networks, Sci. Total Environ. 726 (2020) 138477.
[27] T. Karras, T. Aila, S. Laine, J.J.a.p.a. Lehtinen, Progressive growing of gans for improved quality, stability, and variation, in: International Conference on Learning Representations, 2017.
[28] X. Peng, S. Dasgupta, G. Zhong, M. Du, H. Xu, M. Chen, S. Chen, K. Ta, J. Li, Large debris dumps in the northern South China Sea, Mar. Pollut. Bull. 142 (2019) 164–168.
[29] G. Zhong, X. Peng, Transport and accumulation of plastic litter in submarine canyons—the role of gravity flows, Geology 49 (5) (2021) 581–586.
[30] P. Zhang, L. Ren, X. Zhang, Y. Shan, Y. Wang, Y. Ji, H. Yin, W.E. Huang, J. Xu, B. Ma, Raman-activated cell sorting based on dielectrophoretic single-cell trap and release, Anal. Chem. 87 (4) (2015) 2282–2289.
[31] K. De Gussem, J. De Gelder, P. Vandenabeele, L. Moens, The Biodata toolbox for MATLAB, Chemometr. Intell. Lab. Syst. 95 (1) (2009) 49–52.
[32] K.G. Hartmann, R.T. Schirrmeister, T.J.a.p.a. Ball, EEG-GAN: Generative Adversarial Networks for Electroencephalograhic (EEG) Brain Signals, 2018 arXiv preprint arXiv:1806.01875.
[33] A.L. Maas, A.Y. Hannun, A.Y. Ng, Rectifier Nonlinearities Improve Neural Network Acoustic Models, 2013.
[34] D.P. Kingma, J.J.a.p.a. Ba, Adam, A method for stochastic optimization, in: Proceedings of the 3rd International Conference of Learning Representation, 2014. San Diego.
[35] K. He, X. Zhang, S. Ren, J. Sun, Deep residual learning for image recognition, in: Proceedings of the IEEE Conference on Computer Vision and Pattern Recognition, 2016, pp. 770–778.